The electrical characterization and response to hydrogen of Schottky diodes with a resistive metal electrode—rectifying an oversight in Schottky diode investigation

The electrical characterization and response to hydrogen of Schottky diodes with a resistive metal electrode—rectifying an oversight in Schottky diode investigation

2011 J. Phys. D: Appl. Phys. 44 125101

(http://iopscience.iop.org/0022-3727/44/12/125101)

J. Phys. D: Appl. Phys. **44** (2011) 125101 (9pp) doi:10.1088/0022-3727/44/12/125101

The electrical characterization and response to hydrogen of Schottky diodes with a resistive metal electrode—rectifying an oversight in Schottky diode investigation

P Dawson[1], L Feng[1], L Penate-Quesada[1], J Mitra[3] and G Hill[2]

[1] Centre for Nanostructured Media, School of Maths and Physics, Queen's University of Belfast, Belfast BT7 1NN, UK
[2] EPSRC National Centre for III–V Technologies, Mappin Street, University ofSheffield, Sheffield S1 3JD, UK

E-mail: P.dawson@qub.ac.uk

Received 28 October 2010, in final form 24 January 2011
Published 10 March 2011
Online at stacks.iop.org/JPhysD/44/125101

Abstract
Schottky-barrier structures with a resistive metal electrode are examined using the 4-point probe method where the probes are connected to the metal electrode only. The observation of a significant decrease in resistance with increasing temperature (over a range of ∼100 K) in the diode resistance–temperature (R_D–T) characteristic is considered due to charge carrier confinement to the metal electrode at low temperature (high resistance), with the semiconductor progressively opening up as a parallel current carrying channel (low resistance) with increasing temperature due to increasing thermionic emission across the barrier. A simple model is constructed, based on thermionic emission at quasi-zero bias, that generates good fits to the experimental data. The negative differential resistance (NDR) region in the R_D–T characteristic is a general effect and is demonstrated across a broad temperature range for a variety of Schottky structures grown on Si-, GaAs- and InP-substrates. In addition the NDR effect is harnessed in micro-scaled Pd/n-InP devices for the detection of low levels of hydrogen in an ambient atmosphere of nitrogen.

(Some figures in this article are in colour only in the electronic version)

1. Introduction

The Schottky diode is a fundamental component in solid state electronics and has received extensive attention over the decades since the pioneering work of Mott and Schottky in 1938. The intrinsic potential barrier or Schottky barrier (SB) in this type of device constitutes a rectifying contact and its properties underpin various areas of application [1]. Building on the already vast deployment of Schottky diodes, some more recent and current developments highlight their advantageous features. The very fast response time, combined with the very low reverse-bias leakage current leads to consideration of Schottky diodes as THz sources [2], sensors [3] and modulators [4] for high bandwidth communications. Likewise the Schottky-barrier metal–oxide–semiconductor field-effect transistor (SB-MOSFET) offers advantages over the conventional MOSFET with doped semiconductor source and drain due to suppression of leakage current (I_{off}) and consequent improvement on the order of $\sim 10^4$ in the I_{on} : I_{off} ratio [5–7]. Other intrinsic features such as the high stability and long lifetime have led, for example, to

[3] Current address: Physics Department, Indian Institute of Science Education and Research (IISER), Trivandrum, India.

the adoption of Schottky field-emission sources as the electron source of choice in electron microscopy [8].

The Schottky-barrier height (SBH) varies considerably in magnitude with different metal/semiconductor combinations, ranging from ∼200 meV or even lower to greater than 1 eV [1]. This is an important issue for photodetection where the barrier height defines the long wavelength cut-off for the device. The SB enjoyed a good run for a period as the basis for mid-infrared array detectors [9, 10] on account of the extremely good uniformity of the detection elements despite the poor efficiency of only a few per cent [11]. The most successful of this family was the PtSi/p-Si detector which, with a SBH of ∼225 meV, was very well suited to detection in the 3–5 μm atmospheric transmission window that is key to military and other applications. The reason for specific mention of this SB-based infrared detection technology is that the metal electrode (PtSi) is extremely thin, typically only a few nm thick, determined by the very short mean free path of the photo-excited carriers in the PtSi which have to reach the barrier for the device to operate [12]. In the work reported here the devices depend on the deposition of a very thin, resistive metal electrode and it is interesting to note that such ultra-thin-film technology has been routine in at least one area of Schottky device application. Extension of the infrared detection window to a wavelength of 10 μm or more, exploiting the IrSi/p-Si SB attracted attention for a time [13, 14] but did not take off to the same extent. At the other end of spectral range, and somewhat more recently, modification of the SBH in Au/ZnO-nanoparticle structures upon exposure to ultraviolet radiation appears to play an important role is this 'visible-blind' ultraviolet detection scheme [15].

The SBH itself has been the focus of much attention across the whole gamut of Schottky contacts. It should not be regarded as a fixed, uniform quantity and, indeed, a distribution in the SBH within a given contact offers a physical basis for understanding the introduction of empirical quantities such as the ideality factor in the analysis of current–voltage–temperature (I–V–T) characteristics [16–19]. In particular, the role of molecules at the metal/semiconductor interface in modifying the SBH [20] has been a focus of research attention and is the basis for gas sensing by Schottky diodes [21–24]. As a lead-in to an important aspect of the investigation reported here we specifically highlight the area of hydrogen detection by III–V based Schottky diodes [24–32].

In recent years SB research has been largely materials driven. Attention has been primarily focused on the semiconductor side of the barrier where Schottky contacts based, for example, on SiC [33, 34], GaN [35] and ZnO [36] have all been the subject of extensive investigation. This is particularly the case when the semiconducting materials are in nanostructured format, such as GaN nanowires [37], ZnO nanorods [38], InP nanoneedles [39] and carbon nanotubes [40, 41]. With regard to the barrier region itself, we have already flagged studies on its modification in the context of gas (hydrogen) sensing. On the other hand, the adjoining metal side of the barrier has received relatively little scrutiny, except where it involves a 'metal' of a topical nature, such as graphite [42] or graphene [43, 44] or perhaps a metal that is nanostructured [31]. However, the present investigation is methodology driven, rather than materials driven, thus the use of more 'standard' semiconductors and metals suffices to illustrate the main goals. Also, in contrast to the bulk of the field, much emphasis falls on the metal electrode which we describe as 'resistive', meaning that it is of greater resistance than a portion of the underlying semiconductor of similar lateral dimensions. It is the relative resistance that is important and, as we shall see, the absolute value of the metal-electrode resistance can lie anywhere in the range of a few Ω to several kΩ.

In addition to the deliberate fabrication of very thin, resistive metal electrodes this study differs from the usual mode of SB investigation in that the current delivery and potential difference measurement are made via contacts to the metal electrode only—not via a separate metallic Ohmic contact on the structure. When measurement of the diode resistance, R_D, derived from the 4-point probe to the metal electrode, is conducted as a function of temperature then a significant decrease in R_D is observed with increasing temperature over a limited range—this negative differential resistance (NDR) region in the R_D–T characteristic is shown in figure 1 for various diode structures and will be discussed in more detail below. This type of result is not without precedent in the literature, but it crops up only very occasionally [45, 46] and sometimes almost incidentally [45]; however, as far as we are aware, it has not been investigated, quantitatively analysed or exploited in a methodical fashion. The occurrence of this oversight in the field is perhaps the result of the almost constant coincidence of two factors. Firstly, in nearly all Schottky diodes the metal electrode is quite thick (>100 nm), so even if the 4-probe measurement to only the metal electrode is used, the NDR region in the R_D–T curve is totally masked. Secondly, measurements are nearly always taken directly across the SB to avail of its rectifying properties.

The devices pursued here relate to the introductory comments in a number of ways. In the first place the paradoxical feature is that device operation depends on thermally induced 'leakage' across the barrier, a feature that is generally regarded as undesirable and therefore suppressed in, for example, infrared detection [9, 10]. Nonetheless, the SB characteristics remain crucially important in determining the exact form of the R_D–T curve and so the methodology used here may prove to be a useful SB characterization technique that complements standard I–V ($-T$) and C–V measurements. Equally, since the SBH is sensitive to species reaching the metal/semiconductor interface, this should be reflected in the R_D–T measurements in the configuration that we adopt here—which is indeed the case. In addition to the basic electrical characterization which has been conducted mostly on large-area test samples we present results on hydrogen sensing on prototype thin-film-Pd/n-InP devices where the Pd electrode has been configured as a strip with a large length-to-width ratio in order to increase its resistance. Finally, on a more general point, the resistive metal-electrode scenario developed here is quite generic in nature (any metal electrode can be deposited thin enough to be resistive) and thus may offer a useful additional route to investigate and exploit Schottky diodes especially in the context of nano-scaling.

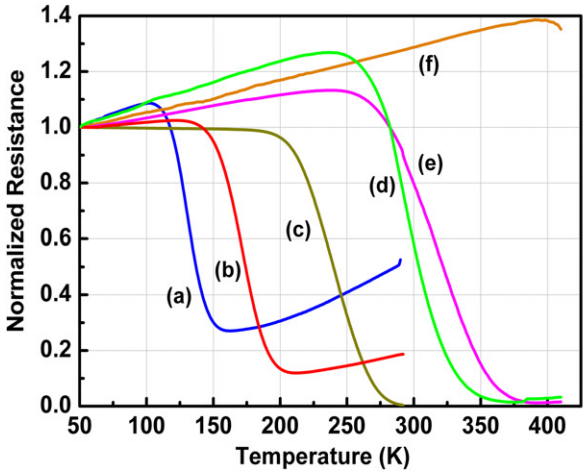

	Schottky Barrier	Source	T_c (K)	SBH (meV)
(a)	PtSi (8 nm)/p-Si	QUB	135	185
(b)	Pd (12 nm)/p-Si	NC3-5T	175	261
(c)	Pd (12 nm)/n-InP	NC3-5T	250	412
(d)	Ag (15 nm)/n-InP	TNI	300	475
(e)	Pt (10 nm)/n-InP	TNI	320	502
(f)	Pt (10 nm)/n-GaAs	TNI	N/A	N/A

Figure 1. Plots of resistance versus temperature, normalized to resistance at 50 K, where the resistance is measured by the 4-point probe method with probes contacted to metal electrode of Schottky sample. Accompanying key and table specifies type of Schottky structure, source of fabrication (QUB—Queen's University Belfast; NC3-5T–EPSRC National Centre for III–V Technologies, University of Sheffield; TNI - Tyndall National Institute, Cork, Ireland), T_c the mid-temperature of the NDR region and the SBH at T_c determined from fits of modelled data to the experimental curves (see figure 2).

2. Experiment

The purpose of the experimental work is two-fold. This first objective is to show, using the methodology outlined above, that the R_D–T characteristics change significantly as a function of SBH over a range of different metal/semiconductor samples, with the mid-temperature of the NDR region, T_c, covering a large temperature range. These data are taken from large-area 'calibration' samples; a more detailed study of patterned Pd/p-Si and PtSi/p-Si devices will be reported separately. The calibration samples are so-called since a series of several such samples was produced for each diode type in order to determine an appropriate metal thickness before committing to the multi-step process of full device fabrication. The second objective is to demonstrate that these resistive-electrode Schottky diodes, configured in the manner described, can act as highly sensitive gas sensors and to this end we present data relating to hydrogen detection by a Pd/n-InP device.

Samples were prepared on both Si and III–V semiconductor substrates in three different laboratories. First, considering the large-area, calibration samples, the PtSi/p-Si sample was prepared in-lab at Queen's University Belfast (QUB) while the Pd/p-Si sample was made in the EPSRC National Centre for III–V Technologies (NC3-5T) at the University of Sheffield (in a departure from their usual work on III–V materials); the Ag/n-InP, Pt/n-InP and Pt/GaAs samples were all prepared in the Compound Semiconductor Laboratory in the Tyndall National Institute (TNI), Cork, Ireland. Like the Pd/p-Si calibration samples the Pd/n-InP devices used in the hydrogen detection part of the work were fabricated in the NC3-5T.

In all cases the semiconductor substrate was moderately to relatively heavily doped in order to offer a low resistance, but not so heavily doped that there was a risk of forming an Ohmic contact. In the case of the III–V semiconductors, where the substrate wafer was heavily doped ($>10^{18}\,\mathrm{cm}^{-3}$), preparation involved the growth of a buffer layer, followed by the growth of a final epilayer prior to metal deposition. The characteristics of the various substrates were as follows: the Si(1 0 0) substrate (QUB) was p-doped (boron) and specified by the manufacturer as having a resistivity in the range 1–5 Ω cm, corresponding to doping density, N_A, in the range $(0.3–1.5) \times 10^{16}\,\mathrm{cm}^{-3}$; a Si(1 0 0) wafer from the same batch was supplied by QUB to NC3-5T for the Pd/p-Si calibration samples; the n-InP substrate (NC3-5T) consisted of a wafer of doping density, $n \sim 4.0 \times 10^{18}\,\mathrm{cm}^{-3}$ with a 500 nm thick buffer layer with $n = 8.5 \times 10^{17}\,\mathrm{cm}^{-3}$ and a 200 nm epilayer with $n = 9.0 \times 10^{16}\,\mathrm{cm}^{-3}$ where the doping densities were determined from electrochemical C–V measurements; the InP substrate from TNI had wafer, buffer layer (500 nm) and epilayer (200 nm) doping densities $\sim 3 \times 10^{18}\,\mathrm{cm}^{-3}$, $\sim 10^{18}\,\mathrm{cm}^{-3}$ and $\sim 3.5 \times 10^{17}\,\mathrm{cm}^{-3}$, respectively. For the p-Si substrate standard cleaning procedures were followed to remove any organic residues and the native oxide was removed using buffered HF ($HF:H_2O = 1:10$) solution prior to deposition of the Pt (Pd) electrode in an electron beam evaporator. To complete the PtSi/p-Si sample the Pt covered substrate was thermally annealed at a temperature of 600 °C for 20 min to form the silicide layer. In the case of the III–V substrates metal deposition took place in-vacuo on the as-prepared epilayers using either electron beam (Pt, Pd) or thermal (Ag) evaporation. In the case of the samples prepared at NC3-5T the metal electrode was further treated by the deposition and subsequent removal by buffered wet etch of a ~100 nm thick layer of Si_3N_4. This was to mimic the process of full device fabrication in which lift-off patterning necessitated this deposition-removal step. Normally, on thicker metal electrodes such post-etching is of little consequence since it may affect (e.g. roughen) only the top few nm of the metal—but here such an affected depth is a much larger fraction of the electrode thickness and so assumes a far greater importance. Also in the case of the NC3-5T samples the processing extended to the formation of an Ohmic contact (InGe/Au bilayer) on the backside of the wafer which facilitated complementary, conventional I–V–T

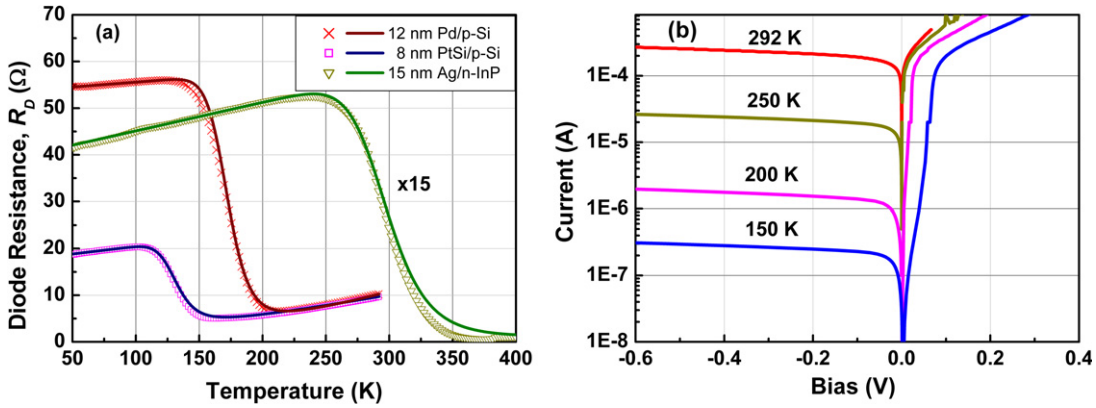

Figure 2. (*a*) Plots of R_D versus temperature, where the resistance is measured by the 4-point probe method with probes contacted to metal electrode of Schottky sample. Symbols are experimental data points and solid lines are modelled curves. (*b*) Current–voltage (I–V) curves for Pd/p-Si Schottky sample at temperatures indicated on the graph; measurements taken in conventional manner across the Schottky structure via Ohmic back contact and Pd electrode on the front surface of the sample.

measurements. Finally, from the several samples of each type made, it was found that the optimum metal-electrode thickness lay in the range 5–15 nm, depending on metal type. The requirement was to have an electrode that offered a resistance of several Ω to several tens of Ω or more, but that was comfortably above the electrical percolation threshold in order to avoid expensive null-yield processing runs at the device fabrication stage. The small thickness of the metal electrode compared with that of the semiconductor substrate 'compensates' for the contrast in resistivities, yielding the semiconductor as an element of resistance comparable to or less than that of the metal electrode and thus a path for significant current flow if the two are placed in competition.

For the 4-point probe measurements the probes were placed in spring loaded contact with the large-area samples on an approximate $4 \times 4\,\mathrm{mm}^2$ footprint with a small piece of indium metal between the probe and the Schottky metal electrode to ensure good electrical contact. To perform the R_D–T measurements the samples were mounted on the cold finger of a CTI Cryotronics closed-cycle helium refrigerator (model 22) equipped with a Lakeshore temperature controller and a programmable source meter HP4000A. The cryostat was designed to cover the temperature range from ∼15 K to ambient; however, a small lab-built heater stage was incorporated in order to extend the temperature range to just above 400 K which was necessary to fully characterize some of the samples. The upper temperature limit was determined by the melting temperature of the solder used by the manufacturer in the cryostat. The R_D–T measurements on the calibration samples were conducted using a digital multi-meter (HP 3457A) operating with HP-VEE virtual instrument software. A current of 1 mA was delivered to the sample while the potential difference recorded between the two voltage probes typically lay in the range 1–100 mV. In cases where the samples also had an Ohmic back contact, conventional I–V–T measurements were taken using an HP3245A current source and the HP3457A digital multi-meter.

The hydrogen detection rig comprised a small, evacuable, UHV 6-way cross fed with hydrogen at the requirement concentration in nitrogen ambient at a constant rate of 2000 sccm. The input gas was sourced from a cylinder of pure nitrogen and one of a hydrogen/nitrogen mixture—this was 2% or 0.1% hydrogen concentration for input concentrations in the ranges 1% to 20 ppm and below 500 ppm, respectively. The input concentration was controlled by MKS 1179A mass flow controllers.

3. Results and discussion

3.1. Electrical characterization

Figure 1 shows plots of resistance as a function of temperature, where the resistance has been normalized to the value at $T = 50$ K. For samples where the NDR region is fully developed at lower temperatures the data end at ambient temperature. Subsequently, for other samples (Pt/n-InP, Ag/n-InP) where T_c is close to ambient, the small, lab-built heater stage was deployed to extend the temperature range above ambient. The data in the accompanying key to figure 1 specify the SB type and T_c, as well as the values of SBH used in fitting modelled R_D–T curves to the experimental data (see later). The main feature to note at this stage is the correlation between the temperature range of the NDR region (and T_c) and the SBH. The value of T_c varies from 135 K for the PtSi/p-Si sample to over 400 K in the case of the Pt/n-GaAs sample where the turn-over in the R_D–T curve is just evident at ∼390 K; however, the limited temperature range curtails full development of the NDR region, frustrating determination of T_c and any meaningful curve fitting. The point is that the NDR feature is quite general and will occur for any type of Schottky contact if the metal electrode is sufficiently resistive.

Figure 2(*a*) shows modelled R_D–T curves and the corresponding experimental data for three cases, PtSi/p-Si, Pd/p-Si and Ag/n-InP. Although the low temperature, metal-electrode resistance differs by a factor of ∼15–20 across these samples the NDR effect is significant in all cases. Indeed, it is the sample (Ag/n-InP) with the lowest value of low-temperature resistance that displays the greatest contrast between maximum and minimum resistance values (factor of 90) across the temperature range—to re-iterate the key factor

is the resistance of the metallic layer relative to that of the substrate, as is evident in the explanation of the results and model that follows.

Conventional I–V curves, based on measurements across the SB between an Ohmic back contact and the top metal electrode, were also recorded as a function of temperature where possible, e.g. in the case of the Pd/p-Si sample in figure 2(*b*). The I–V–T data were fitted using the standard thermionic emission equation for current in a Schottky diode to derive a value for the SBH at each temperature at which results were taken. A quasi-linear increase of SBH with temperature was found, in agreement with other reports in the literature [47, 48], and is described here with an equation of the form

$$\phi_{\mathrm{B}}(T) = \phi_{300\,\mathrm{K}}(1 + \beta(T - 300)), \tag{1}$$

where $\phi_{300\,\mathrm{K}}$ is the SBH at $T = 300$ K and β is the temperature coefficient for the barrier height; for the case of the Pd/p-Si sample of figure 2(*b*), $\beta = 2.9 \times 10^{-4}\,\mathrm{K}^{-1}$. The linear dependence of $\phi_{\mathrm{B}}(T)$ on temperature, which may be regarded as an empirical means of describing inhomogeneity in the barrier [47, 48], was incorporated in the modelling of the R_{D}–T curves. Its inclusion was found to be important in determining the gradient and thus the temperature range of the NDR region. In cases where there was no Ohmic back contact on the sample to facilitate independent determination, a constant temperature coefficient, β, of this magnitude was treated as a free fitting parameter. The values of SBH given with figure 1 are those used in the modelling of the R_{D}–T curves and are cited for $T = T_{\mathrm{c}}$. We note that there tends to be some discrepancy between the value of SBH derived from the fitting and those determined independently from I–V–T measurements (261 meV and 238 meV, respectively, at T_{c} for the case of the Pd/p-Si samples here); later comment on the value of β is pertinent to this point.

A basic understanding of the R_{D}–T curves is straightforward and serves as the basis for constructing a model to describe them quantitatively. At low temperature the carriers in the metal electrode are confined to that electrode and the R_{D}–T characteristic in this regime is therefore that of a metal, essentially linear with a small, positive temperature coefficient. Within a thermionic emission model it can be appreciated that as the temperature increases the carriers can cross the SB and flow via the semiconductor substrate. This mechanism can proceed with increasingly greater probability as the temperature increases. If the resistance of the semiconductor substrate is comparable to or less than that of the metal electrode then, at high temperature, conduction via the semiconductor will be significant and may even dominate. A region of NDR then occurs between the low-temperature regime of conduction exclusively via the metal electrode and the high temperature regime of significant or even dominant conduction via the semiconductor substrate; the temperature of the NDR regime is determined by the SBH, with 'low' and 'high' temperature being purely relative to T_{c}. Of course, in the normal SB set-up the process of conduction between the metal and the semiconductor assumes an applied bias; the effective barrier height presented to the carriers depends both on the magnitude and polarity of the applied bias, yielding the classic rectification behaviour. In the present set-up, however, no bias is applied explicitly across the barrier and the potential difference recorded between the voltage probes is of the order of only a few tens of meV. This is an important consideration in the modelling.

A simple model of a Schottky diode operated in the mode yielding the results of figure 1 comprises of elements of metal-electrode resistance in series and a parallel set of elements of semiconductor resistance also connected in series. These sets of elemental resistances are cross-connected in a resistance network or ladder via the SB resistance, R_{SB}, expressed as

$$R_{\mathrm{SB}} = \frac{C}{J_{\mathrm{o}}} = \frac{C}{A^{*}T^{2}\,\exp(-(q\phi_{\mathrm{B}}(T)/kT))}, \tag{2}$$

where J_{o} is the reverse saturation current density, A^{*} the effective Richardson constant, k the Boltzmann constant, q the carrier charge and C is a temperature-independent proportionality constant. This is the zero-bias form of the expression, meaning that the effective SB resistance, R_{SB}, is driven purely by the thermal energy term, kT. No voltage term appears, in keeping with the fact that only a very small potential difference is developed between the contact electrodes on the sample. (The potential difference per section will become infinitesimally small as the number of elemental sections of the sample increases in the calculation.) The above expression for the effective SB resistance is used along with the appropriate expressions for the resistance elements of the metal electrode and of the semiconductor substrate to yield model R_{D}–T curves. However, it turns out that for the case of large-area calibration samples only a single section or cell of the network is necessary to give a reasonably good approximation to the experimental data. In effect, this amounts to the metal-electrode resistance connected in parallel with the SB and semiconductor resistances connected in series. In this case the diode resistance (for the case of a p-type semiconductor) is simply

$$\frac{1}{R_{\mathrm{D}}} = \frac{1}{R_{\mathrm{o}} + \alpha T} + \frac{1}{R_{\mathrm{SB}} + g/(ep\mu_{\mathrm{h}})}, \tag{3}$$

where the metal-electrode resistance is $R_{\mathrm{o}} + \alpha T$ with R_{o} being the projected zero-temperature resistance and α being the temperature coefficient of resistance. The resistance of the semiconductor element is given by the term $g/(ep\mu_{\mathrm{h}})$ where p is the hole density, μ_{h} the hole mobility and g a geometrical factor, L/A_{S}, where L is the metal-electrode length and A_{S} is the semiconductor cross-section beneath the metal electrode. The model, and resulting single-cell equation (3), addresses only dc operation of the diode and so capacitive components need not be considered. Within equation (3) the detailed evaluation of μ_{h} and p is based on equations in standard texts [1, 49] or the literature [50]:

$$\mu_{\mathrm{h}}(T) \approx \mu_{\mathrm{h}(300\,\mathrm{K})}\left(\frac{300}{T}\right)^{\gamma} \tag{4}$$

$$p = N_{\mathrm{A}}\left[1 + g_{\mathrm{A}}\,\exp\left(\frac{E_{\mathrm{A}} - E_{\mathrm{F}}}{kT}\right)\right]^{-1} + N_{\mathrm{C}}\,\exp\left(-\frac{E_{\mathrm{C}} - E_{\mathrm{F}}}{kT}\right), \tag{5}$$

Table 1. Values of the various metal and semiconductor parameters, as defined in the text, used to produce fits to the diode resistance–temperature (R_D–T) curves for the calibration samples, as shown in figure 2.

	Sample		
Parameters	Ag/n-InP	PtSi/p-Si	Pd/p-Si
$N_{A(D)}$ (10^{15} cm^{-3})	350	9.62	10.6
γ	1.0	2.05	2.46
μ (cm^2 V^{-1} s^{-1})	4600	421	406
R_o (Ω)	2.61	17.2	53.5
α (10^{-3} Ω K^{-1})	4.1	32.4	21.2
$\phi_{300\,K}$ (meV)	475	206	271
β (10^{-4} K^{-1})	5.2	6.2	2.9

where the previously undefined quantities are the temperature scaling exponent of the mobility, γ, the ground state degeneracy factor for acceptor levels, g_A, the acceptor energy level, E_A, the Fermi level, E_F, the conduction band energy level, E_C, the effective density of states in the conduction band, N_C, and the acceptor impurity concentration, N_A. The fits to the experimental data shown in figure 2(a) have been generated using equation (3); perhaps surprisingly the proportionality constant is unity and no further scaling factor on the semiconductor component of the resistance is required. Apart from the various energy levels and g_A, the best-fit parameters for the modelled curves presented in figure 2(a) are given in table 1, including N_A (or N_D, the donor doping density for n-type semiconductors), on which p (or the electron density, n) depend, and the value of the SBH at $T = 300$ K, $\phi_{300\,K}$. It can be seen that the model R_D–T curves replicate the experimental data very well, except in the vicinity of the turning points. This is a satisfactory outcome given the simplicity of equation (3) and the fact that the experimental data cover a range of up to two orders of magnitude between maximum and minimum resistance on a given curve. The modelling can be refined by including multiple units of the resistance network ladder—this cannot be done analytically but may be implemented numerically and is more necessary in relation to devices with elongated metal electrodes formed using standard photolithography; the full development of such modelling will be reported separately.

There are two further points in relation to figure 1. The R_D–T curve for the Pt/n-InP sample has a less negative gradient in the NDR region relative to the nearby curve for the Ag/n-InP sample. This type of R_D–T curve is probably due to a more significant spatial variation in SBH which, in the context of the analysis presented here, is manifest as a larger SB temperature coefficient, β. As an adjunct, the type of R_D–T analysis and modelling discussed above could be used to characterize SB contacts, especially in the initial stages of metal deposition. However, it should be noted that rigorous extension of the model to the case of inhomogeneous barriers is not trivial. Secondly, the R_D–T curve for the Pt/n-GaAs sample exhibits only the start of turn-over towards the NDR region at ~390 K, close to the highest temperature we could attain within the cryostat rig, indicating a rather greater SBH than for the other samples. For Schottky diodes with a resistive metal electrode measured in the 4-probe configuration described, the NDR effect should be perfectly general. The only caveat is that for many typical diodes with barriers in the 800–900 meV range, the corresponding T_c will lie in the range 625–675 K which might imply thermally induced barrier modification.

In concluding our consideration of the electrical properties of these resistive-metal-electrode Schottky samples we note several points. Firstly, T_c and the temperature range of the NDR region ΔT_{NDR} may be determined in principle by selecting a SB of the desired height; the usual array of methods for modification of the barrier height of a given metal/semiconductor combination may be employed. Secondly, the magnitude of the resistance change across the NDR region, ΔR_{NDR}, may be controlled by both the resistance of the metal electrode and that of the semiconductor substrate; this is a regime of control of diode characteristics that has no direct equivalent in standard I–V(–T) measurements across the SB. For the case of a highly resistive metal electrode contacted with a relatively heavily doped semiconductor substrate, ΔR_{NDR} can span at least two orders of magnitude, even for large-area calibration samples; this is before patterning the metal electrode to increase its aspect ratio and thus its resistance (see section 3.2). Conversely, if the metal electrode is too thick and its resistance becomes insignificant relative to the semiconductor substrate, then the NDR behaviour is (completely) suppressed. Finally, it is clearly possible to view these diodes as temperature sensors with extremely high sensitivity over a limited temperature range.

3.2. Hydrogen detection

The high sensitivity of the 4-probe resistance measurements to temperature has been demonstrated. Equally, there should be high sensitivity to change in the barrier properties at fixed (say ambient) temperature provided the barrier change probes the NDR region of the R_D–T characteristic [51]. Thus, for example, if the starting position on the R_D–T curve is just to the low-temperature side of the NDR region, then any lowering of barrier height will cause a collapse in R_D as the NDR region shifts to a lower temperature regime. Schottky diodes based on III–V semiconductors, with a Pd electrode, are known to exhibit sensitivity to hydrogen [25–28, 31]. On interaction with Pd, hydrogen dissociates and becomes chemisorbed in the Pd, forming α- or β-phase Pd hydride [52, 53]. In addition, however, hydrogen diffuses to the barrier region where it forms a dipole layer leading to an effective lowering of the SBH [28]. Taking this information in combination with the NDR effect yields the prospect of sensitive hydrogen detection using the methodology deployed here.

For the hydrogen detection work, patterned devices with an elongated metal electrode were used–such a device is illustrated in cross-section in figure 3(a) with an optical micrograph shown in juxtaposition in figure 3(b). At this point we note that in forming smaller scale device structures the NDR region generally shifts to higher temperatures compared with the case of the corresponding calibration sample—this is the case for the device considered here, where the onset of the NDR region occurs above 350 K (as shown in figure 3(c)) and T_c lies beyond the temperature measurement range, similar to

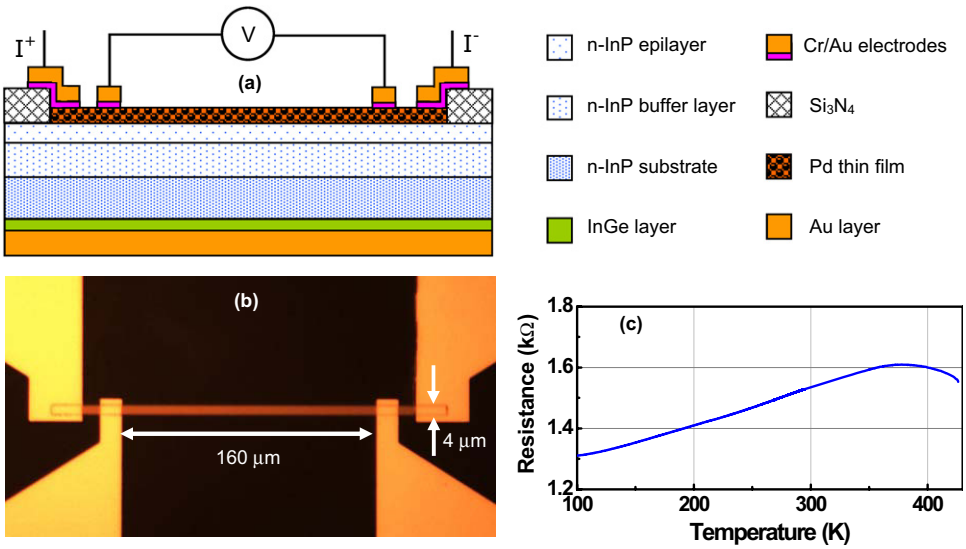

Figure 3. (*a*) Cross-sectional diagram of Pd/n-InP Schottky diode used for hydrogen detection, drawn in juxtaposition to optical micrograph of actual device, (*b*). (*c*) Resistance–temperature plot where resistance is measured by the 4-point probe method shown in parts (*a*) and (*b*), i.e. probes contacted to only Pd electrode of device which is of width 4 μm and length 160 μm between the two inner voltage probe contacts.

the Pt/n-GaAs sample of figure 1. Arguably, the reason for the shift is modification of the semiconductor surface during the lift-off processing that is used to form the devices. There may be a small barrier layer incorporated at the semiconductor–metal interface, yielding a device that conforms more to an MIS structure. The additional resistance associated with such a layer shifts the NDR region to higher temperatures; consequently, application of a thermionic emission-based model to fit the R_D–T curve yields an elevated estimate for the SBH. In any case, the fortuitous nature of the R_D–T curve of figure 3(*b*) offers the possibility of ambient-temperature hydrogen detection which would not be the case for a device exhibiting the R_D–T characteristic of the Pd/n-InP calibration sample of figure 1.

Proceeding with devices of the type shown in figure 3 in the hydrogen exposure set-up, two sets of data from diodes from the same wafer are illustrated in figure 4, covering different hydrogen concentration regimes: 0.1–0.4% (figure 4(*a*)) and the 20–100 ppm range (figure 4(*b*)). We emphasize that these data differ from those of previous work on Schottky diode hydrogen detection in that the measured signal is derived from the 4-point probe method where the contacts are to the (resistive) Pd electrode alone. In thinking about how these results relate to previous Schottky diode-based hydrogen detectors we consider the response time, sensitivity and other features. First of all, the initial time response is slow, as is the case with some other investigations using Schottky diodes [31, 32, 54], and even some work on hydrogen detection using Pd nanoparticles and thin films [55], but once the detector has been 'sensitized' the response to subsequent changes in hydrogen level is somewhat faster, on the scale of minutes. There are two aspects to the slow initial response, the first being that hydrogen must reach the SB interface region where it interacts to cause a lowering of the barrier. The second is that with the NDR region of the device starting somewhat above ambient temperature at zero hydrogen exposure, the SB has to be lowered fairly significantly before a reduction in resistance is detected; in other words, the initial phase of the barrier lowering is not picked up.

The second principal consideration is that of sensitivity. The graph of figure 4(*a*) shows a resistance change 20–30 Ω for 0.1% incremental changes in the ambient hydrogen concentration after the initial drop from ∼1500 Ω to ∼1030 Ω on exposure to an atmosphere with 0.1% hydrogen. These subsequent resistance drops correspond to a sensitivity of $\sim 0.025 \pm 0.005\ \Omega\ \text{ppm}^{-1}$ which may not seem very promising for detection down to the 10 ppm level or lower. However, figure 4(*b*) shows sensitivity in the range 0.7–0.9 $\Omega\ \text{ppm}^{-1}$ after initial exposure to 20 ppm hydrogen concentration. Thus, the absolute sensitivity apparently improves towards lower hydrogen concentrations. In an earlier generation of work on Schottky diode hydrogen sensing, a change of $\sim 10^3$ was reported in forward bias current on exposure to 154 ppm H_2 in N_2 ambient [56]; however, one cannot extrapolate from this result to potential ppm sensitivity since the sensitivity is not a linear function of H_2 concentration; indeed, the trend is for decreasing sensitivity with decreasing hydrogen concentration, [27, 28, 57] in contrast to the dependence reported here. Our current research effort is geared to determining the ultimate hydrogen sensitivity of the device configuration of figure 3 and addressing its variation as a function of hydrogen concentration. For the present it is noted that the device operates as an effective hydrogen detector with a low-end sensitivity that appears to be at least as good as any reported previously. Moreover, only a simple 4-probe measurement of resistance is involved which, because of the device configuration, does not run the risk of current run-off at constant bias that would occur in standard Schottky device measurement with diminishing SBH upon hydrogen exposure.

There are a few further points in relation to figure 4. First, there is recovery to the original resistance reading after cessation of hydrogen exposure, albeit on a long time scale

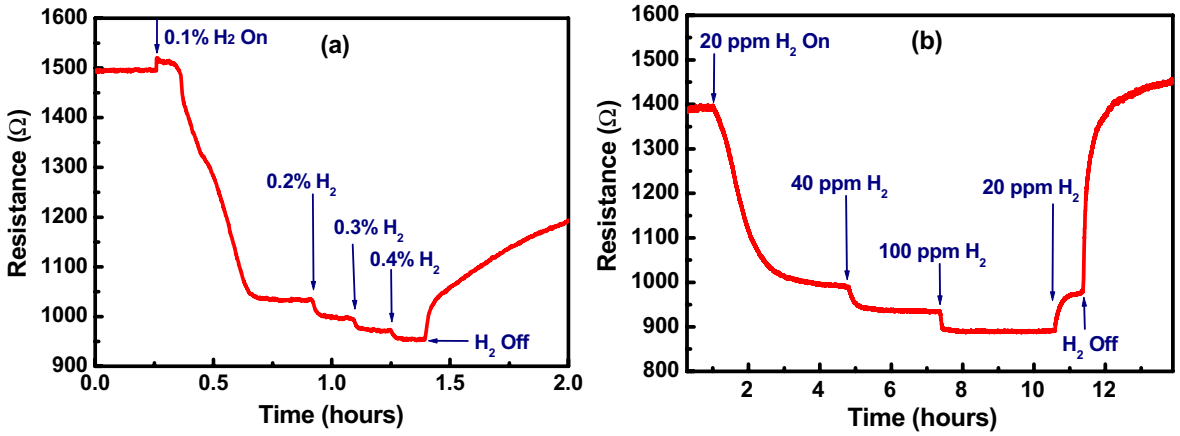

Figure 4. (*a*) Resistance of Pd/n-InP devices of type shown in figure 3 (set-up as shown in figure 3(a)) as a function of hydrogen concentration in the range (*a*) 0.1–0.4% and (*b*) 20–100 ppm.

(figure 4(*b*)). (As an aside it should be noted that in figure 4(*b*) the graph was taken from a series of hydrogen exposure tests where full device recovery had not taken place by the start of the data set.) Secondly, the small upward blip in resistance at a time of ∼0.25 h in figure 4(*a*) is assumed to be due to the response of the Pd electrode alone. This fast, relatively low-sensitivity (∼0.025 Ω ppm^{-1}) response to a high level (0.1%) of hydrogen is a very useful complementary feature to the slow, high-sensitivity response of the SB itself—0.5 Ω ppm^{-1} in the initial resistance drop of figure 4(*a*) or 0.7–0.9 Ω ppm^{-1} sensitivity of figure 4(*b*). Indeed, so far as a practical hydrogen detection scheme is concerned it would be useful to deposit an identical Pd electrode on the insulator (Si_3N_4) adjacent the Schottky device and monitor its resistance separately for the short time-scale detection of higher levels of hydrogen, above say 0.04%, i.e. 1% of the hydrogen flash point in air. In addition, subtracting the Schottky diode response from the isolated Pd strip resistance would yield a sensitive hydrogen sensing signal from the Schottky device against a (near) zero background. A parallel, comparator Schottky device on the same chip, but sealed from the environment, could also be used for temperature compensation if necessary.

4. Conclusion

In conclusion, it has been demonstrated that Schottky diodes with very thin, resistive metal electrodes display a significant NDR region in the R_D–T characteristic that is derived from 4-probe measurements where the contacts are to the metal electrode only. This scheme offers the advantage that the magnitude of the resistance change may be controlled through variation of the resistance of the metal electrode and of the semiconductor substrate which are, in turn, determined by the metal film thickness (and deposition conditions, etc) and the semiconductor doping density, respectively; this contrasts with the given fixed I–V characteristic derived from the usual cross-barrier measurement. A simple model has been constructed that adequately reproduces the form of the R_D–T curves over a range of sample types that display a wide range in the transition temperature, T_c. In addition, the effective operation of resistive-Pd/n-InP devices as hydrogen sensors has been demonstrated in the configuration deployed here and is currently being further explored. The purpose of this paper has been to demonstrate the efficacy of the described methodology in relation to producing NDR in the electrical characteristics across a range of SB interfaces and, in the case of one device type, its application to hydrogen sensing.

Acknowledgments

The authors gratefully acknowledge the support of Proof of Concept grant PoC18A from Invest Northern Ireland, pump-primer funding from the EPSRC (grant ref. GR/G000433) and support from the National Access Programme (Project NAP 140) at the Tyndall National Institute (Cork, Ireland) that provided for fabrication of the Ag/InP, Pt/InP and Pt/GaAs samples in the Compound Semiconductor Laboratory, headed by John Pike. They are also appreciative of advice and encouragement from the Knowledge Exploitation Unit at QUB. LP-Q thanks QUB for studentship support.

References

[1] Sze S M and Ng K K 2007 *Physics of Semiconductor Devices* (Hoboken, NJ: Wiley)
[2] Maestrini A, Ward J, Chattopadhyay G, Schlecht E and Mehdi I 2008 *Frequenz* **62** 118–22
[3] Sizov F 2010 *Opto-Electron. Rev.* **18** 10–36
[4] Chen H T, Padilla W J, Zide J M O, Gossard A C, Taylor A J and Averitt R D 2006 *Nature* **444** 597–600
[5] Calvet L E, Wheeler R G and Reed M A 2002 *Appl. Phys. Lett.* **80** 1761–3
[6] Larson J M and Snyder J P 2006 *IEEE Trans. Electron Devices* **53** 1048–58
[7] Moon R J, Jeong M I, Chandra S V, Shim K H, Jang M, Hong H B, Chang S Y and Choi C J 2009 *J. Electrochem. Soc.* **156** H621–H4
[8] Swanson L W and Schwind G A 2009 *Advances in Imaging and Electron Physics* vol 159 (San Diego, CA: Elsevier Academic Press Inc) pp 63–100
[9] Murguia J E, Mooney J M and Ewing W S 1990 *Opt. Eng.* **29** 786–94
[10] Norton P R 1991 *Opt. Eng.* **30** 1649–63

[11] Norton P and Radford W 1991 *Semicond. Sci. Technol.* **6** C96–C8
[12] Cabanski W A and Schulz M J 1991 *Infrared Phys.* **32** 29–44
[13] Tsaur B Y, Weeks M M, Trubiano R, Pellegrini P W and Yew T R 1988 *IEEE Electron Device Lett.* **9** 650–3
[14] Tsaur B Y, McNutt M J, Bredthauer R A and Mattson R B 1989 *IEEE Electron Device Lett.* **10** 361–3
[15] Jin Y Z, Wang J P, Sun B Q, Blakesley J C and Greenham N C 2008 *Nano Lett.* **8** 1649–53
[16] Werner J H and Guttler H H 1991 *J. Appl. Phys.* **69** 1522–33
[17] McCafferty P G, Sellai A, Dawson P and Elabd H 1996 *Solid-State Electron.* **39** 583–92
[18] Tung R T 2001 *Mater. Sci. Eng.* R **35** 1–138
[19] Chand S and Bala S 2005 *Appl. Surf. Sci.* **252** 358–63
[20] Haick H, Ambrico M, Ligonzo T, Tung R T and Cahen D 2006 *J. Am. Chem. Soc.* **128** 6854–69
[21] Hunter G W, Neudeck P G, Gray M, Androjna D, Chen L Y, Hoffman R W, Liu C C and Wu Q H 2000 *Mater. Sci. Forum* **338–342** 1439–42
[22] Pearton S J, Ren F, Wang Y L, Chu B H, Chen K H, Chang C Y, Lim W, Lin J S and Norton D P 2010 *Prog. Mater. Sci.* **55** 1–59
[23] Salehi A and Nikfarjam A 2004 *Sensors Actuator* B **101** 394–400
[24] Schalwig J, Muller G, Ambacher O and Stutzmann M 2001 *Phys. Status Solidi* a **185** 39–45
[25] Kang W P and Gurbuz Y 1994 *J. Appl. Phys.* **75** 8175–81
[26] Liu W C, Pan H J, Chen H I, Lin K W and Wang C K 2001 *Japan. J. Appl. Phys. Part 1* **40** 6254–9
[27] Chen H I and Chou Y I 2003 *Semicond. Sci. Technol.* **18** 104–10
[28] Chen H and Chou Y 2004 *Semicond. Sci. Technol.* **19** 39–44
[29] Kimura T, Hasegawa H, Sato T and Hashizume T 2006 *Japan. J. Appl. Phys. Part 1* **45** 3414–22
[30] Lee C T and Yan J T 2010 *Sensors Actuator* B **147** 723–9
[31] Chou Y I, Chen C M, Liu W C and Chen H I 2005 *IEEE Electron Device Lett.* **26** 62–5
[32] Wang Y L, Ren F, Zhang U, Sun Q, Yerino C D, Ko T S, Cho Y S, Lee I H, Han J and Pearton S J 2009 *Appl. Phys. Lett.* **94** 212108
[33] Singh R, Cooper J A, Melloch M R, Chow T P and Palmour J W 2002 *IEEE Trans. Electron Devices* **49** 665–72
[34] Eriksson J, Weng M H, Roccaforte F, Giannazzo F, Leone S and Raineri V 2009 *Appl. Phys. Lett.* **95** 081907
[35] Hashizume T, Kotani J and Hasegawa H 2004 *Appl. Phys. Lett.* **84** 4884–6
[36] Allen M W, Weng X J, Redwing J M, Sarpatwari K, Mohney S E, von Wenckstern H, Grundmann M and Durbin S M 2009 *IEEE Trans. Electron Devices* **56** 2160–4
[37] Kim J R, Oh H, So H M, Kim J J, Kim J, Lee C J and Lyu S C 2002 *Nanotechnology* **13** 701–4
[38] Park W I, Yi G C, Kim J W and Park S M 2003 *Appl. Phys. Lett.* **82** 4358–60
[39] Strupeit T, Klinke C, Kornowski A and Weller H 2009 *Acs Nano* **3** 668–72
[40] Heinze S, Tersoff J, Martel R, Derycke V, Appenzeller J and Avouris P 2002 *Phys. Rev. Lett.* **89** 106801
[41] Avouris P, Appenzeller J, Martel R and Wind S J 2003 *Proc. IEEE* **91** 1772–84
[42] Tongay S, Schumann T and Hebard A F 2009 *Appl. Phys. Lett.* **95** 222103
[43] Sonde S, Giannazzo F, Raineri V, Yakimova R, Huntzinger J R, Tiberj A and Camassel J 2009 *Phys. Rev.* B **80** 241406
[44] Li X M, Zhu H W, Wang K L, Cao A Y, Wei J Q, Li C Y, Jia Y, Li Z, Li X and Wu D H 2010 *Adv. Mater.* **22** 2743–8
[45] Oto K, Takaoka S, Murase K and Ishida S 1994 *J. Appl. Phys.* **76** 5339–42
[46] Kojima D, Makihara K, Shi J and Hashimoto M 2001 *Appl. Surf. Sci.* **169** 320–4
[47] Kumar A A, Janardhanam V, Reddy V R and Reddy P N 2009 *Superlatt. Microstruct.* **45** 22–32
[48] Reddy M B, Kumar A A, Janardhanam V, Reddy V R and Reddy P N 2009 *Curr. Appl. Phys.* **9** 972–7
[49] Tyagi M S 1991 *Introduction to Semiconductor Materials and Devices* (New York: Wiley)
[50] Jacoboni C, Canali C, Ottaviani G and Quaranta A A 1977 *Solid-State Electron.* **20** 77–89
[51] Dawson P 2010 *UK Patent* Application No P100762.GB.01
[52] Tabib-Azar M, Sutapun B, Petrick R and Kazemi A 1999 *Sensors Actuator* B **56** 158–63
[53] Dong W, Ledentu V, Sautet P, Eichler A and Hafner J 1998 *Surf. Sci.* **411** 123–36
[54] Cheng C C, Tsai Y Y, Lin K W, Chen H I, Hsu W H, Chuang H M, Chen C Y and Liu W C 2004 *Semicond. Sci. Technol.* **19** 778–82
[55] Joshi R K, Krishnan S, Yoshimura M and Kumar A 2009 *Nanoscale Res. Lett.* **4** 1191–6
[56] Ruths P F, Ashok S and Fonash S J 1981 *IEEE Trans. Electron Devices* **28** 1003–9
[57] Lin K W, Chen H I, Lu C T, Tsai Y Y, Chuang H M, Chen C Y and Liu W C 2003 *Semicond. Sci. Technol.* **18** 615–9